◆ Human Brain Mapping 34:3411–3425 (2013) ◆

Prediction of Alzheimer's Disease and Mild Cognitive Impairment Using Cortical Morphological Patterns

Chong-Yaw Wee, Pew-Thian Yap, and Dinggang Shen; for the Alzheimer's Disease Neuroimaging Initiative

Image Display, Enhancement, and Analysis (IDEA) Laboratory, Biomedical Research Imaging Center (BRIC), Department of Radiology, University of North Carolina at Chapel Hill, North Carolina, USA

Abstract: This article describes a novel approach to extract cortical morphological abnormality patterns from structural magnetic resonance imaging (MRI) data to improve the prediction accuracy of Alzheimer's disease (AD) and its prodromal stage, i.e., mild cognitive impairment (MCI). Conventional approaches extract cortical morphological information, such as regional mean cortical thickness and regional cortical volumes, independently at different regions of interest (ROIs) without considering the relationship between these regions. Our approach involves constructing a similarity map where every element in the map represents the correlation of regional mean cortical thickness between a pair of ROIs. We will demonstrate in this article that this correlative morphological information gives significant improvement in classification performance when compared with ROI-based morphological information. Classification performance is further improved by integrating the correlative information with ROI-based information via multi-kernel support vector machines. This integrated framework achieves an accuracy of 92.35% for AD classification with an area of 0.9744 under the receiver operating characteristic (ROC) curve, and an accuracy of 83.75% for MCI classification with an area of 0.9233. In differentiating MCI subjects who converted to AD within 36 months from non-converters, an accuracy of 75.05% with an area of 0.8426 under ROC curve was achieved, indicating excellent diagnostic power and generalizability. The current work provides an alternative approach to extraction of high-order cortical information from structural MRI data for prediction of neurodegenerative diseases such as AD. *Hum Brain Mapp 34:3411–3425, 2013.* © 2012 Wiley Periodicals, Inc.

Key words: Alzheimer's disease (AD); mild cognitive impairment (MCI); magnetic resonance imaging (MRI); cortical thickness; multi-kernel support vector machine (SVM)

Data used in preparation of this article were obtained from the Alzheimer's Disease Neuroimaging Initiative (ADNI) database (available at: adni.loni.ucla.edu). As such, the investigators within the ADNI contributed to the design and implementation of ADNI and/or provided data but did not participate in analysis or writing of this report. A complete listing of ADNI investigators can be found at: http://adni.loni.ucla.edu/wp-content/uploads/how_to_apply/ADNI_Acknowledgement_List.pdf.

Contract grant sponsor: NIH; Contract grant numbers: EB006733, EB008374, EB009634, MH088520.

*Correspondence to: Dinggang Shen, Department of Radiology and BRIC, University of North Carolina at Chapel Hill, NC 27599. E-mail: dgshen@med.unc.edu

Received for publication 17 January 2012; Revised 25 May 2012; Accepted 2 June 2012

DOI: 10.1002/hbm.22156

Published online 28 August 2012 in Wiley Online Library (wileyonlinelibrary.com).

INTRODUCTION

Alzheimer's disease (AD) is a progressive, irreversible neurodegenerative disease characterized by the decline of cognitive and memory functions, which are serious enough to interfere daily life. This ultimately fatal brain dementia causes certain types of nerve cells in particular areas of the brain to degenerate and die for currently unknown reasons. AD is the most common type of dementia, which accounts for 50% to 80% of dementia cases. Definitive diagnosis of AD can only be made with histopathological confirmation of amyloid plaques and neurofibrillary tangles, usually at autopsy. It has been reported that the incidence of AD doubles every 5 years after age of 65 [Bain et al., 2008] and 1 in every 85 persons will be affected by the disease by year 2050 [Brookmeyer et al., 2007]. The average life expectancy of AD patients varies between 3 and 10 years, depending on the age they are diagnosed with AD. The median life span is as long as 7 to 10 years for AD patients whose conditions are diagnosed when they are in their 60s and early 70s, to only about 3 years or less for patients whose conditions are diagnosed when they are in their 90s [Zanetti et al., 2009].

Mild cognitive impairment (MCI) is an intermediate stage between the expected cognitive decline of normal aging and the more pronounced decline of dementia. It involves problems with memory, language, thinking, and judgment that are greater than typical age-related changes. These problems are severe enough to be noticeable to other people and to show up on tests, but are not serious enough to interfere with daily life. Since the problems do not interfere daily life, the person does not meet the criteria for being diagnosed with dementia. MCI increases the risk of developing dementia, including AD, especially when memory loss is the predominant symptom. This type of MCI is commonly referred as "amnestic MCI." Recent studies show that individuals with MCI tend to progress to probable AD at a rate of approximately 10% to 15% per year [Grundman et al., 2004; Misra et al., 2009], compared with healthy controls who develop dementia at a rate of 1% to 2% per year [Bischkopf et al., 2002]. As life expectancy increases, there is a pressing need for accurate diagnosis of AD at its early stage to enable possible delay of transition from MCI to AD via medications as well as non-medication approaches.

The cerebral cortex is organized into a complex network of local circuits and long-range fiber pathways such as visual network, language network, limbic system, and default network. Interregional interactions between specialized encephalic systems enable different cortical networks to function complementarily. Some studies suggested that functional specialization can also lead to related anatomical variation, such as enlargement of hippocampus size [Maguire et al., 2000, 2003], and enlargement of primary motor and sensorimotor areas, premotor areas, anterior superior parietal areas, and the inferior temporal gyrus [Gaser and Schlaug, 2003a,b; Schlaug, 2001]. In addition, a plethora of studies suggested that the anatomical and functional brain structures experience significant alterations because of pathological attacks, including AD. Specifically, evidence derived from neuropathological, electrophysiological, and neuroimaging studies suggested that the decline of cognitive and memory functions in AD patients was caused by the alterations in functional integration of distributed brain system or structural disconnection between regions due to white matter damage [Delbeuck et al., 2003]. Neurophysiological and neuroimaging studies suggest that AD-associated abnormalities involve not only the functional connection of several specific encephalic regions such as the prefrontal [Grady et al., 2001, 2003; Horwitz et al., 1987], hippocampus [Celone et al., 2006; Wang et al., 2006], cingulate [Greicius et al., 2004], and visual regions [Bokde et al., 2006; Horwitz et al., 1995], but also the functional integration of the entire brain network [Stam et al., 2006, 2007]. There is also growing body of evidence suggesting that AD is associated with the disruption of white matter integrity in regions such as corpus callosum, superior longitudinal fasciculus, and cingulum [Medina et al., 2006; Rose et al., 2000], supramarginal gyrus and putamen [Bozzali et al., 2010], insula and rectue gyrus [Wee et al., 2011].

Many neuroimaging techniques have been applied for AD and MCI detection, including structural magnetic resonance imaging (MRI) [Fan et al., 2008; McEvoy et al., 2009], diffusion tensor imaging (DTI) [Haller et al., 2010; Wee et al., 2011], functional MRI (fMRI) [Machulda et al., 2009; Pihlajamaki and Sperling, 2008; Wee et al., 2012a], positron emission tomography (PET) [Grady et al., 2003; Silveira et al., 2010], and the combination of DTI and resting-state fMRI [Wee et al., 2012b]. Recently, Jack et al. [2010] reported that structural abnormalities can be observed in the human brain before any clinical symptom, indicating that structural abnormalities can be utilized for early detection of AD. Most existing MCI and AD classification frameworks that are based on morphometric data essentially utilize one of the following features: hippocampus features [Cuingnet et al., 2011; Gerardin et al., 2009; Li et al., 2007; Wolf et al., 2001], tissue probability maps [Kloppel et al., 2008; Magnin et al., 2008], and cortical thickness data [Cuingnet et al., 2011; Desikan et al., 2009; Querbes et al., 2009]. Cuingnet et al. [2011] constructed a classifier by combining the cortical thickness values at all vertices as a feature vector. In contrast, Desikan et al. [2009] and Querbes et al. [2009] utilized the mean cortical thickness values of neuroanatomically parcellated regions as a feature vector.

Cortical thickness estimation performed in vivo via MRI is an important technique for the diagnosis and understanding of the progression of neurodegenerative diseases, such as AD. In this study, we chose to employ gray matter cortical thickness (from the baseline scans) as morphological features for AD prediction via a less explored paradigm: is the correlation of morphological abnormalities across different cortical areas surrogate markers of

pathological attacks, such as those caused AD? We employ correlative morphological information extracted from structural MRI to provide a new family of features for AD and MCI prediction. A similar idea of utilizing correlative cortical thickness has also been introduced by Worsley et al., albeit using an approach that is different from ours (i.e., they used statistical parametric map (SPM) and singular value decomposition) [Worsley et al., 2005]. Furthermore, in their method the correlation between the two vertices is computed across subjects. ROI-based morphological information, i.e., gray matter (GM) and white matter (WM) volumes, and regional mean cortical thickness, is included in the proposed framework to provide extra information for better characterization of anatomical abnormalities associated with AD. Correlative and ROI-based morphological features are integrated via a multi-kernel support vector machine (SVM) to further improve prediction capability.

The rest of the article is organized as follows: Method and Materials furnishes information on the image dataset and the postprocessing pipeline. This is followed by a comprehensive description on how the correlative features can be extracted from the mean cortical thickness of different encephalic regions. Integration between correlative and ROI-based morphological information using multi-kernel SVM is briefly described. Performance of the proposed prediction framework is validated extensively in Experimental Results using the ADNI dataset. Findings and methodological issues of the proposed framework are discussed extensively in Discussion. Conclusion provides some concluding remarks.

METHOD AND MATERIALS

Materials

Data used in this study were obtained from the Alzheimer's Disease Neuroimaging Initiative (ADNI) database (available at: adni.loni.ucla.edu). The ADNI was launched in 2003 by the National Institute on Aging (NIA), the National Institute of Biomedical Imaging and Bioengineering (NIBIB), the Food and Drug Administration (FDA), private pharmaceutical companies, and nonprofit organizations, as a $60 million, 5-year public–private partnership. The primary goal of ADNI has been to test whether serial MRI, PET, other biological markers, and clinical and neuropsychological assessment can be combined to measure the progression of MCI and early AD. Determination of sensitive and specific markers of very early AD progression is intended to aid researchers and clinicians to develop new treatments and monitor their effectiveness, as well as lessen the time and cost of clinical trials. Readers are referred to www.adni-info.org for more information.

The Principal Investigator of this initiative is Dr. Michael W. Weiner, MD, VA Medical Center and University of California, San Francisco. ADNI is the result of efforts of many coinvestigators from a broad range of academic institutions and private corporations, and subjects have been recruited from over 50 sites across the U.S. and Canada. The initial goal of ADNI was to recruit 800 adults, ages 55 to 90, to participate in the research, approximately 200 cognitively normal older individuals to be followed for 3 years, 400 people with MCI to be followed for 3 years, and 200 people with early AD to be followed for 2 years. The key eligibility criteria used in ADNI were described at http://www.adni-info.org/Scientists/ADNIGrant/ProtocolSummary.aspx. According to ADNI clinical procedures, diagnosis of AD was made if the subject had a mini-mental state examination (MMSE) [Folstein et al., 1975] score between 24 and 26 (inclusive), a clinical dementia rating (CDR) [Morris, 1993] of 0.5 or 1.0, and meets NINCDS/ADRDA criteria [McKhann et al., 1984] for probable AD. Individuals were categorized as amnestic MCI if they had a MMSE score between 24 and 30 (inclusive), a memory complaint, objective memory loss measured by education adjusted scores on Wechsler Memory Scale Logical Memory II [Wechsler, 1987], a CDR of 0.5, absence of significant levels of impairment in other cognitive domains, while essentially preserved activities of daily living, and an absence of dementia. On the other hand, all normal control individuals met the following criteria: a MMSE score between 24 and 30 (inclusive), a CDR of 0, nondepressed, non-MCI, and nondemented. The age range of normal subjects will be roughly matched to that of MCI and AD subjects with minimal enrollment under the age of 70. The delayed recall performance in the Alzheimer's Disease Assessment Scale score (ADAS-Cog) 10-Word list [Rosen et al., 1984] was selected from the cognitive measures included in the ADNI database because delayed recall has been shown to be a strong predictor of AD [Estevez-Gonzalez et al., 2003; Rountree et al., 2007].

Five hundred ninety-eight subjects who belong to one of the AD, MCI, or normal control (NC) groups were analyzed in this study. These subjects were selected randomly for a ratio of AD versus MCI versus NC roughly as 1:1:1. All subjects received the baseline clinical/cognitive examinations including 1.5T structural MRI scan, and were reevaluated at specified intervals (6 or 12 months). The baseline scans were used as the input data in our experiments. The follow-up examination results were used to separate MCI subjects into two subcategories, stable MCI (sMCI) and progressive MCI (pMCI). Subjects who converted to AD within 36 months were classified as pMCI, and those not converted to AD within the same period were classified as sMCI. Table I shows the demographic information of the participants involved in this study. The conversion from MCI to AD up to 36 months before clinical criteria of AD are met is provided in Figure 1.

Overview of Methodology

An overview of the proposed AD/MCI classification framework is summarized schematically in Figure 2.

TABLE I. Demographic information of the participants involved in this study

	Diagnosis group			
Variables	NC	sMCI	pMCI	AD
No. subjects (*n*)	200	111	89	198
Gender				
Male	103	83	60	103
Female	97	28	29	95
Age (mean ± SD)	75.8 ± 5.0	75.3 ± 7.3	74.8 ± 6.9	75.7 ± 7.7
Education years (mean ± SD)	15.9 ± 2.9	15.9 ± 3.2	15.9 ± 3.0	14.7 ± 3.1
Cognitive scores				
ADAS-Cog (mean ± SD)	6.1 ± 3.0	10.3 ± 5.0	12.6 ± 3.7	17.3 ± 8.0
MMSE (mean ± SD)	28.6 ± 3.8	25.9 ± 6.1	26.7 ± 1.6	21.8 ± 6.1
CDR (mean ± SD)	0 ± 0.1	0.4 ± 0.3	0.5 ± 0.0	0.6 ± 0.5

NC = normal controls; sMCI = static MCI; pMCI = progressive MCI; AD = Alzheimer's disease.

The proposed framework can essentially be divided into two parts: training and testing. For training, two types of features were extracted from the MR volume of every subject based on the Desikan–Killiany Cortical Atlas [Desikan et al., 2006], which contains 68 gyral-based ROIs, 34 for each hemisphere. The first feature type is the ROI-based morphological features, which consist of the regional mean cortical thickness values, and the cerebral cortical GM, and the cortical associated WM volumes. The second feature type is the correlative features, which are obtained by the similarity of cortical thickness between pairs of ROIs. The Desikan–Killiany Cortical Atlas and the names of ROIs are provided in Figure 3.

To select the discriminative features that are helpful for classification, a hybrid feature selection method was applied separately to the correlative and ROI-based features. Individual kernel matrices were then constructed based on the selected optimal features of each feature type before they were integrated to form a single mixed-kernel matrix via multi-kernel SVM. The constructed mixed-kernel matrix was finally employed to train a SVM classifier via 10-fold cross-validation.

To classify a new test subject, we first extracted the ROI-based features from the subject's MR volumes. We then constructed the correlative features from the regional mean cortical thickness. Individual kernel matrices were constructed for each feature type based on the optimal features selected in the training process. These individual kernel matrices were then integrated to form a mixed-kernel matrix that will act as the input to the previously trained SVM classifier to determine the class to which the new test subject should belong.

ROI-Based Morphological Features

ROI-based morphological features, i.e., regional mean cortical thickness, and cerebral cortical GM and cortical associated WM volumes, were extracted in an automated manner via FreeSurfer software suite (available at: http://surfer.nmr.mgh.harvard.edu/, version 4.5.0). FreeSurfer is a free, popular cortical surface analysis software that can perform effective volumetric segmentation and cortical surface reconstruction [Desikan et al., 2006; Fischl and Dale, 2000; Fischl et al., 1999a,b, 2002]. Once the cortical models were completed, a number of deformable procedures were performed for further data processing and analysis [Desikan et al., 2006; Fischl et al., 1999b, 2004]. Both intensity and continuity information from the entire three-dimensional MR volume are used in segmentation and deformation procedures to produce representations of cortical thickness [Dale et al., 1999; Fischl et al., 1999a). Procedures for the measurement of cortical thickness have been thoroughly validated against histological analysis [Rosas et al., 2002] and manual measurements [Kuperberg et al., 2003; Salat et al., 2004], and demonstrated good test–retest reliability across different scanners and field strengths [Dickerson et al., 2008; Han et al., 2006]. Readers are referred to Dickerson et al. [2008] for detailed explanations regarding cortical surface reconstruction and cortical thickness measurement.

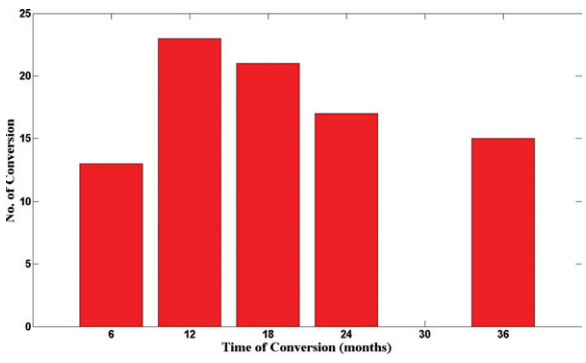

Figure 1.
Conversion from MCI to AD up to 36 months in pMCI subgroup. [Color figure can be viewed in the online issue, which is available at wileyonlinelibrary.com.]

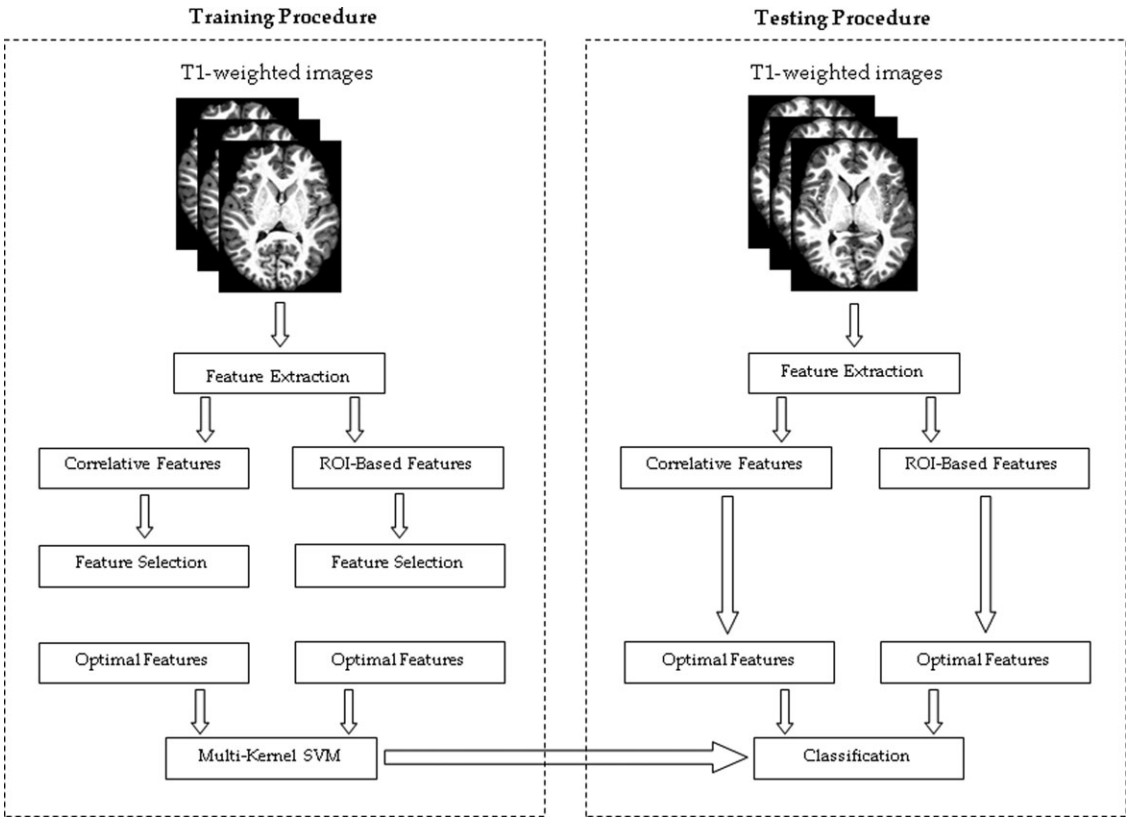

Figure 2.
Schematic overview of the proposed AD/MCI classification framework.

In addition to the regional mean cortical thickness, standard deviation for cortical thickness of each ROI was also computed during the construction of cortical models. In this study, normalized regional mean cortical thickness features were used in the proposed framework by dividing the regional mean cortical thickness of each ROI with

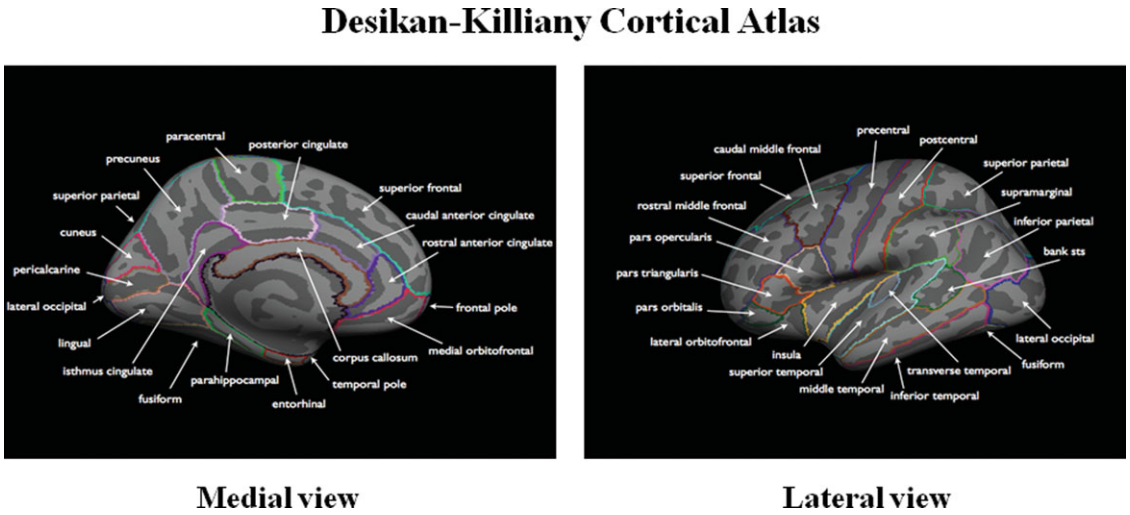

Figure 3.
Desikan–Killiany Cortical Atlas used for brain space parcellation. The medial and lateral views of the atlas are obtained from http://web.mit.edu/mwaskom/pyroi/freesurfer_ref.html. [Color figure can be viewed in the online issue, which is available at wileyonlinelibrary.com.]

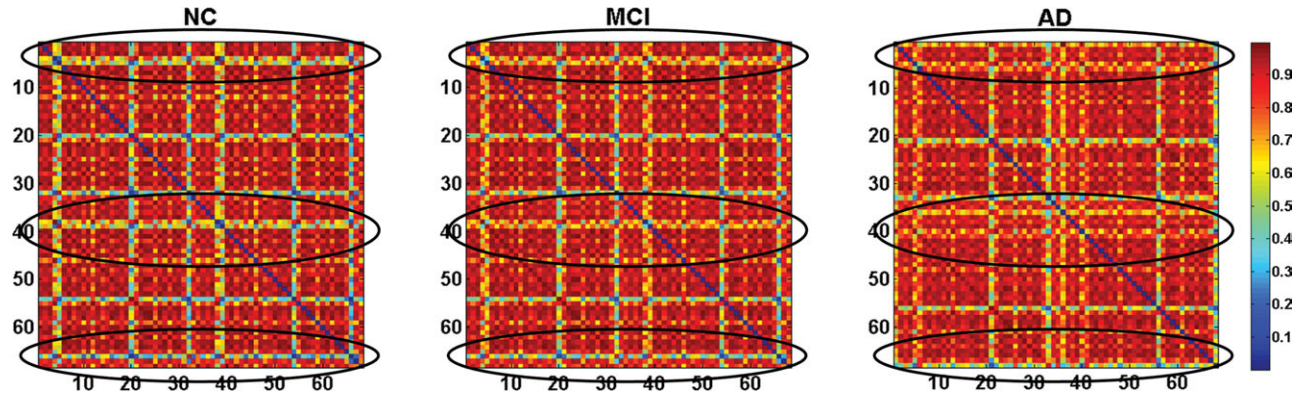

Figure 4.

Population average similarity maps for the NC, MCI, and AD groups. NC and MCI maps are similar, but they are both different from AD map. [Color figure can be viewed in the online issue, which is available at wileyonlinelibrary.com.]

its respective standard deviation. To provide additional morphological description, we also included the regional cortical volumetric information into our proposed framework. We utilized the same ROIs defined in the Desikan–Killiany Cortical Atlas to extract the cerebral cortical GM and cortical associated WM volumes. The intracranial volume (ICV) of every individual was also extracted. Since ICV is unaltered by the disease, normalizing total or regional volumes of each subject by their respective ICV value provides better estimate of brain volume and makes them more comparable [Whitwell et al., 2001]. Therefore, we used the normalized GM and WM volumes of each ROI in this study to provide a more appropriate volumetric representation.

Correlative Morphological Features

It is well known that AD and similar dementias exhibit subtle, spatially and temporally diffuse pathology, where the brain is damaged as a large-scale, highly connected network, rather than in one single isolated region [He et al., 2008; Stam et al., 2007]. In view of this, we designed an interregional description, which might be more sensitive in conveying the pathological information for accurate diagnosis of neurological diseases. In this study, we proposed the application of correlative cortical thickness information between pairs of ROIs for AD/MCI prediction. Using the Desikan–Killiany Cortical Atlas, a (68×68) matrix map was constructed with every element representing the similarity of regional mean cortical thicknesses between a pair of ROIs. The similarity map is symmetric with ones along its diagonal.

Specifically, for the ith and jth regions, the dissimilarity of the cortical thicknesses is defined as

$$d(i,j) = [t(i) - t(j)]^2 \tag{1}$$

where $t(i)$ and $t(j)$ denote the regional mean cortical thickness of regions ith and jth, respectively. The similarity between regions ith and jth was computed as

$$s(i,j) = \exp\left(-\frac{d(i,j)}{2\sigma^2}\right) \tag{2}$$

where $\sigma = \sqrt{\sigma_i + \sigma_j}$ with σ_i and σ_j denoting the standard deviation of regional cortical thickness of regions ith and jth. This new feature type measures the relative morphological abnormalities across different encephalic regions, instead of morphological abnormalities in isolated regions as in conventional methods. It is worth noting that the dissimilarity measure [Eq. (1)] and the similarity measure [Eq. (2)] can be replaced by other functions for similarity map construction. Due to symmetry, only the upper (or lower) triangular of the similarity map was used. For each subject, all similarity values of the upper triangular part of the similarity map were concatenated to form a long feature vector with 2,278 elements ($(N \times (N-1))/2$, with $N = 68$).

The population average similarity map for NC, MCI, and AD groups are shown in Figure 4. Significant topological differences can be observed between the similarity map of NC and AD groups, particularly in the central and boundary regions of the maps as highlighted by black circles. These regions correspond to ROIs such as bankssts, caudal anterior cingulate cortex, caudal middle frontal gyrus, cuneus cortex, entorhinal cortex, superior temporal sulcus, supramarginal gyrus, frontal pole, temporal pole, transverse temporal, and insula. However, topology structure of similarity map between NC and MCI groups are similar and only subtle variations can be observed. These observations are in line with the abnormalities caused by neuropathology, i.e., AD patients experience more significant brain atrophies when compared with NC and MCI groups while

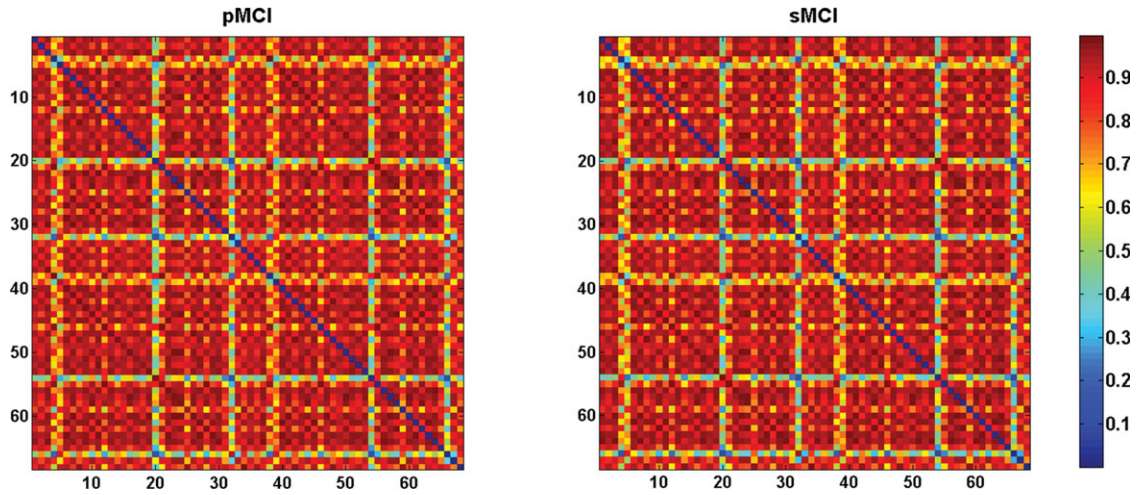

Figure 5.
Population average similarity maps for the pMCI and sMCI subgroups, which look similar to each other. [Color figure can be viewed in the online issue, which is available at wileyonlinelibrary.com.]

the brain atrophies in MCI individuals are subtle and are very similar to NC. The population average similarity maps for pMCI and sMCI subgroups are provided in Figure 5, with no significant difference visually. Also, they are very similar to the MCI and NC groups. Based on two-sample *t*-test performed on every element in the similarity maps, only 11.85% of the total elements show significant differences ($P < 0.05$) between pMCI and sMCI subgroups. This value is much lower than other between-group comparisons, i.e., AD versus NC (64.14%), MCI versus NC (41.09%), and AD versus MCI (48.07%). This might explain why the classification of pMCI from sMCI is much more challenging than other classification tasks.

Feature Selection

Solving pattern recognition or classification problems with data of high dimensionality is a challenging task due to the curse of dimensionality. This is particularly true for neuroimaging classification problems. With the presence of irrelevant or redundant features, learning models tend to overfit and become less generalizable. Feature selection is a useful and important means to identify relevant features for dimensionality reduction and improving generalization performance [Guyon and Elisseeff, 2003; Liu and Yu, 2005]. Due to high dimensionality of the correlative morphological features, we utilized a hybrid feature selection method to select the most relevant features for AD and MCI prediction. Essentially, the feature selection algorithms used in this study comprised two categories, i.e., filter-based and wrapper-based approaches. Filter-based approaches rely on the general characteristics of data to evaluate the features without any learning algorithm, while wrapper-based approaches normally involve a predefined learning algorithm where its performance is used as evaluation criterion for selecting a subset of most discriminative features. In our hybrid approach, two filter-based approaches were initially used to reduce the number of features, followed by a wrapper-based approach to further select a subset of features that was favorable to AD and MCI prediction.

Specifically, in the first filter-based approach, only those features with their P values is smaller than the predefined threshold, measured via between-group *t*-test, will be retained for subsequent feature selection. Despite the reduction in dimensionality, the features retained by this simple approach may still inevitably be intercorrelated. Therefore, we employed another filter-based approach, called minimum redundancy and maximum relevance (mRMR) [Ding and Peng, 2005; Peng et al., 2005], to further reduce the feature dimensionality. The mRMR model provides a balance between two aspects of feature selection, i.e., efficiency and broadness. Efficiency ensures that characteristics can be represented with a minimal number of features without significant reduction in prediction performance. Broadness ensures that the selected feature subset can be the maximally representative of original space covered by the entire dataset. In mRMR, mutual information is used to measure the relevance of every feature pair and between features and classes. Specifically, we minimize the total relevance of feature pairs to achieve minimum redundancy, while simultaneously maximize the total relevance of feature-class pairs to achieve maximum relevance.

An effective wrapper-based model, called the support vector machine recursive feature elimination (SVM-RFE) [Guyon et al., 2004; Rakotomamonjy, 2003], was utilized to further reduce the number of selected features. The selected subset contains features that are most favorable to AD and MCI prediction. The goal of SVM-RFE is to find a subset of size l among d features ($l < d$) which optimizes the performance of the SVM classifier. The basic principle of SVM-RFE is to ensure that the removal of a particular feature will

make the classification error smallest. In this study, we employed SVM with linear kernel to evaluate the discriminative power of the selected features. It is noteworthy that the hybrid feature selection was performed separately on each feature type (i.e., correlative and ROI-based features) as shown in Figure 2. Finally, for each feature type we have an individual optimal feature subset. Before performing feature selection on each feature type, the raw features were first scaled individually to range [−1, +1]. Then, every scaled feature was normalized across all training subjects to obtain its standard score (*z*-value). These steps ensured that the regional mean cortical thickness and ICV normalized volumetric measures were within the same scale, minimizing possible bias that may occur when performing selection on features with different dynamic ranges.

Classification Using Multi-kernel SVM

A multiple-kernel learning framework was applied to construct a set of descriptors from the previously selected feature vectors for improving prediction performance. Specifically, we utilized a multi-kernel SVM with radial basis function (RBF) kernel to integrate information from the correlative and ROI-based morphological features. A kernel matrix was first constructed for each feature type based on RBF kernel before they were integrated using multi-kernel SVM to form a mixed-kernel matrix with the most appropriate weighting factors.

Specifically, given n training samples with $\mathrm{x}_i = \{\mathrm{x}_i^{(1)}, ..., \mathrm{x}_i^{(M)}\}$ denoting the feature vector of the ith sample which contains M types of features and $y_i \in \{-1, 1\}$ the corresponding labels, the multi-kernel SVM of dual form that integrates information from M feature types and forms a mixed-kernel matrix can be given as

$$\max_{\alpha} \sum_{i=1}^{n} \alpha_i - \frac{1}{2} \sum_{i,j} \alpha_i \alpha_j y_i y_j \sum_{m=1}^{M} \beta_m k^{(m)} \left(\mathrm{x}_i^{(m)}, \mathrm{x}_j^{(m)} \right) \qquad (3)$$

s.t. $k^{(m)}(\mathrm{x}_i^{(m)}, \mathrm{x}_j^{(m)}) = \langle \Phi(\mathrm{x}_i^{(m)}), \Phi(\mathrm{x}_j^{(m)}) \rangle$; $\sum_{i=1}^{n} \alpha_i y_i = 0$; with $0 \le \alpha_i \le C,\ i = 1, ..., n$ where $\Phi(\bullet)$ denotes the kernel-induced mapping function, $k^{(m)}(\mathrm{x}_i^{(m)}, \mathrm{x}_j^{(m)})$ denotes the kernel matrix for training samples $\mathrm{x}_i^{(m)}$ and $\mathrm{x}_j^{(m)}$ of the mth feature type, α denotes the Lagrange multiplier, $\langle \bullet, \bullet \rangle$ denotes the inner product, $\beta_m \ge 0$ denotes the weighting factor on the m-th feature type, and C denotes the model parameter that controls the amount of constraint violations. Given a new test sample $\mathrm{x} = \{\mathrm{x}^{(1)}, \ldots, \mathrm{x}^{(M)}\}$, the decision function for label prediction is

$$F(\mathrm{x}) = \mathrm{sign}\left(\sum_{i=1}^{n} \alpha_i y_i \sum_{m=1}^{M} \beta_m k^{(m)}(\mathrm{x}_i^{(m)}, \mathrm{x}^{(m)}) \right) \qquad (4)$$

The optimal SVM model, as well as an unbiased estimation of the generalization performance of the complete framework, was obtained via a nested cross-validation scheme. Specifically, two nested cross-validation loops were employed to accomplish these goals. The inner cross-validation loop was used to determine the hyperparameter of the SVM models from a training set while the outer cross-validation loop was used to evaluate the generalizability of SVM models using an independent validation set. This procedure was performed via a 10-fold cross-validation. SVM model that performed the best during the nested cross-validation stage was considered the optimal model and its hyperparameter will be used to classify new test subjects.

EXPERIMENTAL RESULTS

The discriminative power of the proposed integrated and correlative morphological features were compared with three ROI-based features, i.e., regional mean cortical thickness, regional cortical volumes, and combined ROI-based features. The combined ROI-based features were constructed by concatenating all the regional mean cortical thickness and regional cortical volumes into a long feature vector. The performance of the multi-kernel SVM using the integrated features was compared with the single kernel SVMs using other feature types. For each comparison, performance of every compared method was validated through three different classification tasks: AD versus NC, MCI versus NC, and AD versus MCI. The MCI dataset used was the combination of all the pMCI and sMCI subjects shown in Table I.

As the MCI subjects are well known for their heterogeneity, it is important to categorize MCI subjects into different subgroups for better characterizing cognitive and neural changes during disease progression. We performed the validation based on two MCI subgroups, i.e., pMCI and sMCI. In every experiment, we randomly partitioned the data into two sets, one for training and one for testing, with similar number of subjects from each class in each set. The experiment was repeated 20 times to evaluate the performance of all compared methods by determining their mean classification accuracy, area under receiver operating characteristic curve (ROC), sensitivity, and specificity. The average classification performance estimated using this approach tends to be more conservative than the traditional leave-one-out approach. It also ensures that the trained SVM models are validated with independent test sets for more precise estimation on how accurately they will perform in practice. Details of each experiment are described in the following subsections.

Comparison Between Integrated, Correlative, and ROI-Based Features

In this experiment, performance of the proposed correlative features was compared with the ROI-based features (the regional mean cortical thickness, regional cortical volumes, and hippocampus volumes). The mean classification

TABLE II. Comparison between integrated, correlative, and ROI-based features

	AD vs. NC					MCI vs. NC					AD vs. MCI				
Features	ACC	*P*	SEN	SPE	AUC	ACC	*P*	SEN	SPE	AUC	ACC	*P*	SEN	SPE	AUC
Hippocampus	81.54	<0.0001	0.7692	0.8615	0.8868	72.78	<0.0001	0.6755	0.7800	0.7982	63.46	<0.0001	0.6566	0.6126	0.6871
Thickness	84.65	<0.0001	0.8278	0.8652	0.9175	74.87	<0.0001	0.7332	0.7640	0.8301	72.35	0.0006	0.7131	0.7335	0.8137
Volume	87.40	0.0002	0.8515	0.8965	0.9364	77.00	<0.0001	0.7463	0.7932	0.8528	74.29	0.0003	0.7177	0.7682	0.8265
Combined	89.70	0.0063	0.8758	0.9182	0.9489	79.23	0.0106	0.7630	0.8215	0.8806	74.72	0.0011	0.7364	0.7581	0.8217
Correlative	88.15	0.0002	0.8455	0.9173	0.9535	79.00	0.0001	0.7570	0.8230	0.8856	76.39	0.0230	0.7396	0.8182	0.8617
Integrated	92.35	—	0.9035	0.9431	0.9744	83.75	—	0.8355	0.8395	0.9233	79.24	—	0.7803	0.8046	0.8882

Thickness = regional mean cortical thickness; hippocampus = hippocampus volume; volume = regional cortical volumes; combined = combination of the regional mean cortical thickness and regional cortical volumes; integrated = integration of the correlative and ROI-based features; ACC = ACCuracy; SEN = SENsitivity; SPE = SPEcificity.

accuracy, sensitivity, specificity, and area under ROC curve (AUC) values of each compared feature type were summarized in Table II. We also performed paired *t*-test on the classification accuracy between the integrated features and all other feature types, and the computed *P* values are provided in Table II.

It can be observed that the hippocampus volumes (left and right volume) performed the worst among all compared feature types in all classification tasks due to the insufficient information conveyed by the hippocampus volumes alone. The performance given by the regional mean cortical thickness was also not satisfactory. However, when the correlative features were used, classification performance improved significantly. The proposed integrated morphological approach shows significantly better performance than all other feature types in all statistical measures used for comparison. The small *P* values for classification accuracy indicate the superiority of the integrated morphological features over the other feature types. For difficult classification tasks such as MCI versus NC and AD versus MCI, the proposed framework always shows an area larger than 0.88 under the ROC curve (AUC), indicating excellent diagnostic power. The proposed approach always exhibits much better correct prediction on patients as reflected by its significantly higher sensitivity value.

Classification Between pMCI And sMCI

Separation of MCI individuals into subgroups, i.e., the pMCI and sMCI, is crucial for possibly early treatment and possibly delay of transition of the pMCI subjects to AD. Hence, a good AD/MCI prediction framework must be able to perform this task efficiently. We evaluated the performance of our proposed framework based on the categorized MCI subgroups provided in Table I. The proposed framework was compared with all the methods in the previous subsection and the results are summarized in Table III. Note that the structural images used for discriminating the pMCI and sMCI subjects in this study are the baseline scans.

It can be clearly observed that the proposed framework using the integrated morphological information performs the best in identifying MCI subjects who convert to clinical AD within 36 months. The regional mean cortical thickness performed the worst particularly for the sensitivity and AUC values. However, significant improvement can be observed when the correlative features were used. The classification performance is significantly improved by multi-kernel SVM-based integration of the features.

To further evaluate the robustness of our proposed method for prediction of pMCI subjects at different conversion times, we performed the same classification procedures for pMCI subjects who converted to clinical AD within 36, 24, 18, and 12 months. In the experiments, we used the same number of sMCI as the pMCI subjects at each conversion time to minimize the effects of unbalanced data. The classification performance of pMCI subjects at different conversion time is summarized in Table IV. It can be observed that the proposed method performs reasonably well for earlier conversion prediction. The classification accuracy is greater than 70.0% with AUC values greater than 0.8 for all cases, indicating good generalization performance. It is noteworthy that the sensitivity is always larger than 0.70, while the specificity is around 0.70, indicating relatively robust and balanced classification performance.

TABLE III. Categorized MCI subgroups classification between all compared methods

	pMCI vs. sMCI				
Features	ACC	*P*	SEN	SPE	AUC
Thickness	68.30	<0.0001	0.5614	0.7786	0.7295
Volume	68.20	<0.0001	0.5943	0.7509	0.7629
Combined	71.45	0.0433	0.6011	0.8036	0.8106
Correlative	71.85	0.0041	0.6159	0.7991	0.8320
Integrated	75.05	—	0.6352	0.8441	0.8426

ACC = ACCuracy; SEN = SENsitivity; SPE = SPEcificity.

TABLE IV. Classification of pMCI subjects at different conversion time

Conversion time (mo)	pMCI vs. sMCI			
	ACC	SEN	SPE	AUC
12	71.67	0.7028	0.7306	0.8036
18	70.18	0.7036	0.7000	0.8358
24	71.01	0.7135	0.7068	0.8184
36	71.76	0.7364	0.6989	0.8228

ACC = ACCuracy; SEN = SENsitivity; SPE = SPEcificity.

The Most Discriminative Regions

The discriminative regions that were selected from the proposed classification framework for identifying the MCI converters from nonconverters are reported in Table V. The selected regions for other classification tasks are quite similar and thus not reported due to space limit. The Table V lists the top 20 selected ROI-based and correlative morphological features.

It is found that the selected ROI-based features are from both the regional mean cortical thickness and the regional cortical volumes, indicating the existence of complementary information between these two morphological features. It is also found that the selected features are from both brain hemispheres and all four lobes, indicating the spread of morphological abnormalities over whole brain. Based on the selected features, the ROIs that contribute for good classification performance in the pMCI classification task include the middle temporal gyrus, entorhinal cortex, superior and inferior parietal cortices, fusiform gyrus, bankssts (banks of the superior temporal sulcus), supramarginal gyrus, precuneus cortex, parahippocampal, posterior cingulate cortex, insula, medial orbitofrontal cortex, and pars orbitalis (parts of inferior frontal gyrus).

Based on the selected correlative features, pairs of regions that contribute for classification are not only within the same hemisphere and same lobe but also across different hemispheres and lobes. This indicates that the morphological relation between different areas of the brain, either adjacent or distant, might provide some meaningful information for describing different stages of neurodegenerative disease. Most of the regions that were selected from the correlative features are similar to the regions selected from the ROI-based features. The regions that are selected by both feature types include the middle temporal gyrus, entorhinal cortex, inferior parietal cortex, fusiform gyrus, bankssts, precuneus cortex, insula, and medial orbitofrontal cortex. Other regions that were only selected from the correlative features include the precentral and postcentral gyri, lateral occipital cortex, rostral and caudal middle frontal gyri, caudal anterior cingulate cortex, temporal pole, pars opercularis and pars triangularis (the first and second gyri from the precentral gyrus), isthmus of cingulate cortex, paracentral lobule, pericalcarine cortex, lateral orbitofrontal cortex, cuneus cortex, and superior frontal gyrus.

TABLE V. Top 20 most discriminative ROI-based and correlative morphological features that were selected during multi-kernel SVM training in the pMCI vs. sMCI classification task

No.	ROI-based features	Freq	Correlative features	Freq
1	Entorhinal_R_G	15	Precentral_L–lateral occipital_R	7
2	Bankssts_L_T	12	Superior temporal_L–fusiform_R	6
3	Middle temporal_L_G	11	Rostral middle frontal_L–paracentral_R	5
4	Superior parietal_R_G	11	Caudal anterior cingulate_L–temporal pole_R	5
5	Inferior parietal_L_G	10	Lateral occipital_R–pars triangularis_R	4
6	Entorhinal_L_G	10	Caudal anterior cingulate_R–isthmus cingulate_R	4
7	Supramarginal_R_G	9	Inferior parietal_L–supramarginal_L	4
8	Precuneus_R_G	8	Pericalcarine_L–precuneus_R	4
9	Precuneus_L_G	7	Pars triangularis_R–rostral middle frontal_R	4
10	Inferior temporal_L_G	6	Paracentral_L–lateral occipital_R	4
11	Bankssts_L_G	6	Superior parietal_L–cuneus_R	4
12	Insula_L_G	5	Pericalcarine_L–entorhinal_R	4
13	Inferior temporal_L_T	5	Middle temporal_L–insula_R	4
14	Medial orbitofrontal_R_G	5	Bankssts_L–pars opercularis_R	4
15	Fusiform_R_G	5	Lateral orbitofrontal_L–lateral orbitofrontal_R	3
16	Posterior cingulate_R_T	5	Precentral_L–rostral middle frontal_L	3
17	Entorhinal_L_T	5	Caudal anterior cingulate_L–medial orbitofrontal_R	3
18	Parahippocampal_R_T	5	Superior temporal_L–postcentral_R	3
19	Pars orbitalis_L_G	5	Middle temporal_L–postcentral_R	3
20	Fusiform_R_T	5	Bankssts_R–Superior frontal_R	3

L = left; R = right; G = gray matter; W = white matter; T = thickness; Freq = frequency.

DISCUSSION

In the present study, we introduced a new approach of feature extraction method that extracts correlative morphological information using the regional mean cortical thickness. This information was used to effectively discriminate the MCI and AD patients from normal controls, as well as between the MCI and AD patients. The correlative features give better classification performance than the ROI-based features, such as regional mean cortical thickness and regional volume, in all classification tasks when validated using a large cohort of patients from the ADNI dataset.

To further improve the classification performance, we integrated the correlative and ROI-based features via the multi-kernel SVM. Promising classification results was achieved using the integrated features: 92.35% (AUC = 0.9744), 83.75% (AUC = 0.9233), and 79.24% (AUC = 0.8882) for AD classification, MCI classification, and AD-MCI classification, respectively. High AUC value achieved indicates excellent diagnostic power and generalizability of the proposed framework to unseen dataset. In addition, our framework substantially improves the classification performance, particularly the sensitivity rate, compared with ROI-based morphological feature-based classifiers. These results indicate that the proposed framework can be used to provide additional diagnostic information for early treatment of the disease.

The identification of individuals in the transitional phase is critical for testing disease-modifying therapies and for the development of novel medications to prevent or delay AD, particularly from a clinical and financial perspective, since consistent and frequent follow-up of healthy individuals that might or might not be at risk for AD is extremely difficult, especially in a typical clinical setting. We applied the integrated morphological feature-based SVM classifier to a large number of MCI patients from the ADNI dataset. Our findings demonstrate that the proposed framework can detect subtle structural changes either at individual-region level or across-region level that help to identify those MCI individuals who converted to AD up to 36 months before clinical diagnosis. The predicted accuracy of the conversion of MCI to AD within 36 months is 75.05% with a high AUC value of 0.8426. The classification procedure employed in this study gives a conservative but possibly more accurate estimate of the classification generalizability. The classification between pMCI and sMCI subgroups at different conversion time demonstrated a relatively robust and balanced performance of the proposed framework by providing consistently classification accuracy, AUC, sensitivity, and specificity values.

The brain regions that were selected for accurate detection of AD and MCI patients, as well as the conversion from pMCI to AD have already been extensively reported in previous studies, either in changes of volume or cortical thickness. These included the precuneus cortex and insula [Fan et al., 2008; Misra et al., 2009), orbitofrontal cortex, precuneus cortex and insula [Misra et al., 2009], posterior cingulate gyrus, precuneus cortex and insula [Davatzikos et al., 2011], parahippocampal gyrus [Celone et al., 2006; Machulda et al., 2009; Pihlajamaki and Sperling, 2008], inferior temporal gyrus and precentral gyrus [Lenzi et al., 2011], inferior temporal gyrus, inferior frontal gyrus and insula [Han et al., 2010], entorhinal cortex [Devanand et al., 2007; Du et al., 2001; Pennanen et al., 2004], middle temporal gyrus [Risacher et al., 2009], entorhinal cortex and supramarginal gyrus [Desikan et al., 2009], bankssts, entorhinal cortex, fusiform gyrus, middle temporal gyrus, parahippocampal gyrus, pars orbitalis, pars triangularis, paracentral lobule, postcentral gyrus, rostral middle frontal gyrus and superior parietal cortex [Wang et al., 2009], entorhinal gyrus, parahippocampal gyrus, middle and inferior temporal gyri, precuneus cortex, isthmus of cingulate cortex, posterior cingulate cortex, bankssts, medial and lateral orbitofrontal cortices, rostral and caudal middle gyri, superior frontal gyrus, precentral gyrus, fusiform gyrus, superior and inferior parietal cortices, and supramarginal gyrus [Liu et al., 2011], precuneus and cuneus cortices [Niskanen et al., 2011], temporal gyrus, inferior and superior parietal gyri, and lateral occipital cortex [Liu et al., in press]. The fact that our findings are consistent with results reported in previous studies demonstrates the efficacy of our proposed framework in identifying correct biomarkers for classification purposes.

An interesting finding in present study is that the most selected correlative feature in the sMCI and pMCI classification task is between the left precentral gyrus and right lateral occipital cortex as given in Table V. It is well known that significant anomalies in the left precentral gyrus and right lateral occipital cortex can only be observed in the brain of AD patients, but not in its early stage (MCI). However, the results provided in Table V are for the classification task between sMCI and pMCI subjects. As we know that pMCI subjects have higher tendency of progression to AD, selection of some regions that only experience significant alterations in AD (later stage), but not in MCI (early stage), might favor the classification between sMCI and pMCI. Furthermore, there is more than 40% of pMCI subjects used in the experiment have converted to AD within a relatively short period of time (less than 12 months). This might suggest that some of these pMCI subjects already showed certain degree of anomalies in regions with alterations that can only be observed in AD patients, such as left precentral gyrus and right lateral occipital cortex, as indicated by the present study.

Although the majority of the neuroimaging literature of AD and MCI has focus on measuring morphological abnormalities in individual ROIs, our study suggests that the baseline cortical morphological abnormality patterns between different ROIs across the whole brain can be utilized to increase the prediction accuracy on an individual basis. These correlative morphological abnormality patterns are complex and include regions that are located either adjacent or distant. The methodology presented herein is built around this concept, that is, the

morphological alterations caused by AD and MCI pathological attacks are not restricted to certain brain areas, but widely spread over the whole brain, and the relative changes between pairs of ROIs might convey useful discriminative information. The proposed approach is significantly different from the ROI-based approach, which examine the brain region-by-region independently, without integrating the entire pattern of atrophy [Davatzikos et al., 2005a,b] throughout all brain regions together. This is very important, because although many regions generally display significant group differences, they might also significantly overlap between groups [Fan et al., 2008], and therefore do not provide sufficient sensitivity and specificity for diagnostic purposes. The integration of ROI-based and correlative morphological information provided the best results, suggesting that the correlative features convey additional and somewhat complementary information to the ROI-based features. This fully multivariate approach herein provides a more general and comprehensive way of examining the data.

CONCLUSIONS

In this article, we proposed a new approach of extracting morphological information from structural MRI images. We constructed a regional cortical thickness similarity map for each subject to describe the correlative changes in cortical thicknesses between pairs of ROIs. We demonstrated that this correlative information gives better characterization of structural changes in MCI and AD patients. By integrating the proposed correlated morphological features with the ROI-based morphological features via multikernel SVM, significant improvement in classification performance can be achieved. When applied to discriminate pMCI subjects from sMCI subjects, our proposed classification framework outperformed other methods by providing higher values for all statistical measures used for comparison. The promising results give supportive evidence on the effectiveness of applying correlative cortical information for diagnosis and prediction of progressive neurodegenerative diseases, such as AD.

ACKNOWLEDGMENTS

Data collection and sharing for this project was funded by the Alzheimer's Disease Neuroimaging Initiative (ADNI) (National Institutes of Health Grant U01 AG024904). ADNI is funded by the National Institute on Aging, the National Institute of Biomedical Imaging and Bioengineering, and through generous contributions from the following: Abbott; Alzheimer's Association; Alzheimer's Drug Discovery Foundation; Amorfix Life Sciences Ltd.; AstraZeneca; Bayer HealthCare; BioClinica, Inc.; Biogen Idec Inc.; Bristol-Myers Squibb Company; Eisai Inc.; Elan Pharmaceuticals Inc.; Eli Lilly and Company; F. Hoffmann-La Roche Ltd and its affiliated company Genentech, Inc.; GE Healthcare; Innogenetics, N.V.; Janssen Alzheimer Immunotherapy Research & Development, LLC.; Johnson & Johnson Pharmaceutical Research & Development LLC.; Medpace, Inc.; Merck & Co., Inc.; Meso Scale Diagnostics, LLC.; Novartis Pharmaceuticals Corporation; Pfizer Inc.; Servier; Synarc Inc.; and Takeda Pharmaceutical Company. The Canadian Institutes of Health Research is providing funds to support ADNI clinical sites in Canada. Private sector contributions are facilitated by the Foundation for the National Institutes of Health (www.fnih.org). The grantee organization is the Northern California Institute for Research and Education, and the study is coordinated by the Alzheimer's Disease Cooperative Study at the University of California, San Diego. ADNI data are disseminated by the Laboratory for Neuro Imaging at the University of California, Los Angeles. This research was also supported by NIH grants P30 AG010129, K01 AG030514, and the Dana Foundation.

REFERENCES

Bain LJ, Jedrziewski K, Morrison-Bogorad M, Albert M, Cotman C, Hendrie H, Trojanowski JQ (2008): Healthy brain aging: A meeting report from the Sylvan M. Cohen Annual Retreat of The University of Pennsylvania Institute On Aging. Alzheimers Dement 4:443–446.

Bischkopf J, Busse A, Angermeyer MC (2002): Mild cognitive impairment—A review of prevalence, incidence and outcome according to current approaches. Acta Psychiatr Scand 106:403–414.

Bokde ALW, Lopez-Bayo P, Meindl T, Pechler S, Born C, Faltraco F, Teipel SJ, Moller HJ, Hampel H (2006): Functional connectivity of the fusiform gyrus during a face-matching task in subjects with mild cognitive impairment. Brain 129:1113–1124.

Bozzali M, Parker GJM, Serra L, Embleton K, Gili T, Perri R, Caltagirone C, Cercignani M (2010): Anatomical connectivity mapping: A new tool to assess brain disconnection in Alzheimer's disease. Neuroimage 54:2045–2051.

Brookmeyer R, Johnson E, Ziegler-Graham K, Arrighi HM (2007): Forecasting the global burden of Alzheimer's disease. Alzheimers Dement 3:186–191.

Celone KA, Calhoun VD, Dickerson BC, Atri A, Chua EF, Miller SL, DePeau K, Rentz DM, Selkoe DJ, Blacker D, Albert, MS, Sperling, RA (2006): Alterations in memory networks in mild cognitive impairment and Alzheimer's disease: An independent component analysis. J Neurosci 40:10222–10231.

Cuingnet R, Gerardin E, Tessieras J, Auzias G, Lehericy S, Habert M-O, Chupin M, Benali H, Colliot O, The Alzheimer's Disease Neuroimaging Initiative (2011): Automatic classification of patients with Alzheimer's disease from structural MRI: A comparison o ten methods using ADNI database. Neuroimage 56:766–781.

Dale AM, Fischl B, Sereno MI (1999): Cortical surface-based analysis: I. Segmentation and surface reconstruction. Neuroimage 9:179–194.

Davatzikos C, Acharyya M, Ruparel K, Shen DG, Loughhead J, Gur RC, Langleben D (2005a): Classifying spatial patterns of brain activity for lie-detection. Neuroimage 28:663–668.

Davatzikos C, Bhatt P, Shaw LM, Batmanghelich KN, Trojanowski JQ (2011): Prediction of MCI to AD conversion, via MRI, CSF

biomarkers, and pattern classification. Neurobiol Aging 32:2322.e19–2322.27.

Davatzikos C, Shen DG, Wu X, Lao Z, Hughett P, Turetsky BI, Gur RC, Gur RE (2005b): Whole-brain morphometric study of schizophrenia reveals a spatially complex set of focal abnormalities. JAMA Arch Gen Psychiatry 62:1218–1227.

Delbeuck X, Van der Linden M, Collette F (2003): Alzheimer's disease as a disconnection syndrome? Neuropsychol Rev 13:79–92.

Desikan RS, Cabral HJ, Hess CP, Dillon WP, Glastonbury CM, Weiner MW, Schmansky NJ, Greve DN, Salat DH, Buckner RL, et al. (2009): Automated MRI measures identify individuals with mild cognitive impairment and Alzheimer's disease. Brain 132:2048–2057.

Desikan RS, Segonne F, Fischl B, Quinn BT, Dickerson BC, Blacker D, Buckner RL, Dale AM, Maguire RP, Hyman BT, et al. (2006): An automated labeling system for subdividing the human cerebral cortex on MRI scans into gyral based regions of interest. Neuroimage 31:968–980.

Devanand DP, Pradhaban G, Liu X, Khandji A, De Santi S, Segal S, Rusinek H, Pelton GH, Hoing LS, Mayeux R, et al. (2007): Hippocampal and entorhinal atrophy in mild cognitive impairment. Neurology 68:828–836.

Dickerson BC, Fenstermacher E, Salat DH, Wolk DA, Maguire RP, Desikan R, Pachecoc J, Quinn BT, der Kouwe AV, Greve DN, et al. (2008): Detection of cortical thickness correlates of cognitive performance: Reliability across MRI scan sessions, scanners, and field strengths. Neuroimage 39:10–18.

Ding C, Peng H (2005): Minimum redundancy feature selection from microarray gene expression data. J Bioinform Comput Biol 3:185–205.

Du AT, Schuff N, Amend D, Laakso MP, Hsu YY, Jagust WJ, Yaffe K, Kramer JH, Reed B, Norman D, et al. (2001): Magnetic resonance imaging of the entorhinal cortex and hippocampus in mild cognitive impairment and Alzheimer's disease. J Neurol Neurosurg Psychiatry 71:441–447.

Estevez-Gonzalez A, Kulisevsky J, Boltes A, Otermin P, Garcia-Sanchez C (2003): Rey verbal learning test is a useful tool for differential diagnosis in the preclinical phase of Alzheimer's disease: Comparison with mild cognitive impairment and normal aging. Int J Geriatr Psychiatry 18:1021–1028.

Fan Y, Batmanghelich N, Clark CM, Davatzikos C, the Alzheimer's Disease Neuroimaging Initiative (2008): Spatial patterns of brain atrophy in MCI patients, identified via high-dimensional pattern classification, predict subsequent cognitive decline. Neuroimage 39:1731–1743.

Fischl B, Dale AM (2000): Measuring the thickness of the human cerebral cortex from magnetic resonance images. Proc Natl Acad Sci USA 97:11050–11055.

Fischl B, Salat DH, Busa E, Albert M, Dieterich M, Haselgrove C, van der Kouwe A, Killiany R, Kennedy D, Klaveness S, et al. (2002): Whole brain segmentation: Automated labeling of neuroanatomical structures in the human brain. Neuron 33:341–355.

Fischl B, Salat DH, van der Kouwe AJ, Makris N, Segonne F, Quinn BT, Dale AM (2004): Sequence-independent segmentation of magnetic resonance images. Neuroimage 23(Suppl 1):S69–S84.

Fischl B, Sereno MI, Dale AM (1999a): Cortical surface-based analysis. II: Inflation, flattening, and a surface-based coordinate system. Neuroimage 9:195–207.

Fischl B, Sereno MI, Tootell RBH, Dale AM (1999b): High-resolution intersubject averaging and a coordinate system for the cortical surface. Hum Brain Mapp 8:272–284.

Folstein MF, Folstein SE, McHugh PR (1975): "Mini-mental state". A practical method for grading the cognitive state of patient for the clinician. J Psychiatr Res 12:189–198.

Gaser C, Schlaug G (2003a): Brain structures differ between musicians and non-musicians. J Neurosci 23:9240–9245.

Gaser C, Schlaug G (2003b): Gray matter differences between musicians and nonmusicians. Ann NY Acad Sci 999:514–517.

Gerardin E, Chetelat G, Chupin M, Cuingnet R, Desgranges B, Kim H-S, Niethammer M, Dubois B, Lehericy S, Garnero L, et al. (2009): Multidimensional classification of hippocampal shape features discriminates Alzheimer's disease and mild cognitive impairment from normal aging. Neuroimage 47: 1476–1486.

Grady CL, Furey ML, Pietrini P, Horwitz B, Rapoport SI (2001): Altered brain functional connectivity and impaired short-term memory in Alzheimer's disease. Brain 124:739–756.

Grady CL, McIntosh AR, Beig S, Keightley ML, Burian H, Black SE (2003): Evidence from functional neuroimaging of a compensatory prefrontal network in Alzheimer's disease. J Neurosci 23:986–993.

Greicius MD, Srivastava G, Reiss AL, Menon V (2004): Default-mode network activity distinguishes Alzheimer's disease from healthy aging: Evidence from functional MRI. Proc Natl Acad Sci USA 101:4637–4642.

Grundman M, Petersen RC, Ferris SH, Thomas RG, Aisen PS, Bennett DA, et al. (2004): Mild cognitive impairment can be distinguished from Alzheimer's disease and normal aging for clinical trials. Arch Neurol 61:59–66.

Guyon I, Elisseeff A (2003): An introduction to variable and feature selection. J Mach Learn Res 3:1157–1182.

Guyon I, Weston J, Barnhill S, Vapnik V (2004): Gene selection for cancer classification using support vector machines. Mach Learn 46:389–422.

Haller S, Nguyen D, Rodriguez C, Emch J, Gold G, Bartsch A, Lovblad KO, Giannakopoulos P (2010): Individual prediction of cognitive decline in mild cognitive impairment using support vector machine-based analysis of diffusion tensor imaging data. J Alzheimers Dis 22:315–527.

Han X, Jovicich J, Salat D, van der Kouwe A, Quinn B, Czanner S, Busa E, Pacheco J, Albert M, Killiany R, et al. (2006): Reliability of MRI-derived measurements of human cerebral cortical thickness: The effects of field strength, scanner upgrade and manufacturer. Neuroimage 32:180–194.

Han Y, Wang J, Zhao Z, Min B, Lu J, Li K, He Y, Jia J (2010): Frequency-dependent changes in the amplitude of low-frequency fluctuations in amnestic mild cognitive impairment: A resting-state fMRI study. Neuroimage 55:287–295.

He Y, Chen ZJ, Evans AC (2008): Structural insights into aberrant topological patterns of large-scale cortical networks in Alzheimer's disease. J Neurosci 28:4756–4766.

Horwitz B, Grady CL, Schlageter NL, Duara R, Rapoport SI (1987): Intercorrelations of regional cerebral glucose metabolic rates in Alzheimer's disease. Brain Res 407:294–306.

Horwitz B, McIntosh AR, Haxby JV, Furey M, Salerno JA, Schapiro MB, Rapoport SI, Grady CL (1995): Network analysis of PET-mapped visual pathways in Alzheimer type dementia. Neuroreport 6:2287–2292.

Jack CR Jr, Knopman DS, Jagust WJ, Shaw LM, Aisen PS, Weiner MW, Petersen RC, Trojanowski JQ (2010): Hypothetical model of dynamic biomarkers of the Alzheimer's pathological cascade. Lancet Neurol 9:119–128.

Kloppel S, Stonnington CM, Chu C, Draganski B, Scahill RI, Rohrer JD, Fox NC, Jack CR Jr, Ashburner J, Frackowiak RSJ (2008): Automatic classification of MR scans in Alzheimer's disease. Brain 131:681–689.

Kuperberg GR, Broome MR, Mcguire PK, David AS, Eddy M, Ozawa F, Goff D, West C, Williams SCR, van der Kouwe AJW, et al. (2003): Regionally localized thinning of the cerebral cortex in schizophrenia. Arch Gen Psychiatry 60:878–888.

Lenzi D, Serra L, Perri R, Pantano P, Lenzi GL, Paulesu E, Caltagirone C, Bozzali M, Macaluso E (2011): Single domain amnestic MCI: A multiple cognitive domains fMRI investigation. Neurobiol Aging 32:1542–1557.

Li S, Shi F, Pu F, Li X, Jiang T, Xie S, Wang Y (2007): Hippocampal shape analysis of Alzheimer disease based on machine learning methods. Am J Neuroradiol 28:1339–1345.

Liu H, Yu L (2005): Toward integrating feature selection algorithms for classification and clustering. IEEE Trans Knowledge Data Eng 17:491–502.

Liu Y, Julkunen V, Paajanen T, Westman E, Wahlund LO, Aitken A, Sobow T, Mecocci P, Tsolaki M, Vellas B, Muehlboeck S, Spenger C, Lovestone S, Simmons A, Soininen H, AddNeuroMed Consortium. Education increases reserve against Alzheimer's disease-evidence from structural MRI analysis. Neuroradiology doi: 10.1007/s00234-012-1005-0.

Liu Y, Paajanen T, Zhang Y, Westman E, Wahlund L-O, andd Catherine Tunnard AS, Sobow T, Mecocci P, Tsolaki M, Vellas B, Muehlboeck S, Evans A, Spenger C, Lovestone S, Soininen H, AddNeuroMed Consortium (2011): Combination analysis of neuropsychological tests and structural MRI measures in differentiating AD, MCI and control groups—The AddNeuroMed study. Neurobiol Aging 32:1198–1206.

Machulda MM, Senjem ML, Weigand SD, Smith GE, Ivnik RJ, Boeve BF, Knopman DS, Petersen RC, Jack J, Clifford R (2009): Functional MRI changes in amnestic and non-amnestic MCI during encoding and recognition tasks. J Int Neuropsych Soc 15:372–382.

Magnin B, Mesrob L, Kinkingnehun S, Pelegrini-Issac M, Colliot O, Sarazin M, Dubois B, Lehericy S, Benali H (2008): Support vector machine-based classification of Alzheimer's disease from whole-brain anatomical MRI. Neuroradiology 51:73–83.

Maguire EA, Gadian DG, Johnsrude IS, Good CD, Ashburner J, Frackowiak RSJ, Frith CD (2000): Navigation-related structural change in the hippocampi of taxi drivers. Proc Natl Acad Sci USA 97:4398–4403.

Maguire EA, Spiers HJ, Good CD, Hartley T, Frackowiak RS, Burgess N (2003): Navigation expertise and the human hippocampus: A structural brain imaging analysis. Hippocampus 17:250–259.

McEvoy LK, Fennema-Notestine C, Roddey JC, Hagler DJ Jr, Holland D, Karow DS, Pung CJ, Brewer JB, Dale AM (2009): Alzheimer disease: Quantitative structural neuroimaging for detection and prediction of clinical and structural changes in mild cognitive impairment. Radiology 251:195–205.

McKhann G, Drachman D, Folstein M, Katzman R, Price D, Stadlan EM (1984): Clinical diagnosis of Alzheimer's disease: Report of the NINCDS-ADRDA Work Group under the auspices of Department of Health and Human Services Task Force on Alzheimer's Disease. Neurology 34:939–944.

Medina D, deToledo-Morrell L, Urresta F, Gabrieli JDE, Moseley M, Fleischman D, Bennett DA, Leurgans S, Turner DA, Stebbins GT (2006): White matter changes in mild cognitive impairment and AD: A diffusion tensor imaging study. Neurobiol Aging 27:663–672.

Misra C, Fan Y, Davatzikos C (2009): Baseline and longitudinal patterns of brain atrophy in MCI patients, and their use in prediction of short-term conversion to AD: Results from ADNI. Neuroimage 44:1414–1422.

Morris JC (1993): The clinical dementia rating (CDR): Current version and scoring rules. Neurology 43:2412–2414.

Niskanen E, Kononen M, Maatta S, Hallikainen M, Kivipelto M, Casarotto S, Massimini M, Vanninen R, Mervaala E, Karhu J, et al. (2011): New insights into Alzheimer's disease progression: A combined TMS and structural MRI study. PLoS One 6:e26113.

Peng H, Long F, Ding C (2005): Feature selection based on mutual information: Criteria of max-dependency, max-relevance, and min-redundancy. IEEE Trans Pattern Anal Mach Intell 27:1226–1285.

Pennanen C, Kivipelto M, Tuomainen S, Hartikainen P, Hanninen T, Laakso MP, Hallikainen M, Vanhanen M, Nissinen A, Helkala EL, et al. (2004): Hippocampus and entorhinal cortex in mild cognitive impairment and early AD. Neurobiol Aging 25:303–310.

Pihlajamaki M, Sperling RA (2008): fMRI: Use in early Alzheimer's disease and in clinical trials. Future Neurol 3:409–421.

Querbes O, Aubry F, Pariente J, Lotterie J-A, Demonet J-F, Duret V, Puel M, Berry I, Fort J-C, Celsis P, et al. (2009): Early diagnosis of Alzheimer's disease using cortical thickness: Impact of cognitive reserve. Brain 132:2036–2047.

Rakotomamonjy A (2003): Variable selection using svm based criteria. J Mach Learn Res 3:1357–1370.

Risacher SL, Saykin AJ, West JD, Shen L, Firpi HA, McDonald BC, the Alzheimer's Disease Neuroimaging Initiative (2009): Baseline MRI predictors of conversion from MCI to probable AD in the ADNI cohort. Curr Alzheimer Res 6:347–361.

Rosas HD, Liu AK, Hersch S, Glessner M, Ferrante RJ, van der Kouwe DHSA, Jenkins BG, Fischl AMDB (2002): Regional and progressive thinning of the cortical ribbon in Huntington's disease. Neurology 58:695–701.

Rose SE, Chen F, Chalk JB, Zelaya FO, Strugnell WE, Benson M, Semple J, Doddrell DM (2000): Loss of connectivity in Alzheimer's disease: An evaluation of white matter tract integrity with colour coded MR diffusion tensor imaging. J Neurol Neurosurg Psychiatry 69:528–530.

Rosen WG, Mohs RC, Davis KL (1984): A new rating scale for Alzheimer's disease. Am J Psychiatry 141:1356–1364.

Rountree SD, Waring SC, Chan WC, Lupo PJ, Darby EJ, Doody RS (2007): Importance of subtle amnestic and nonamnestic deficits in mild cognitive impairment: Prognosis and conversion to dementia. Dement Geriatr Cogn Disord 24:476–482.

Salat DH, Buckner RL, Snyder AZ, Greve DN, Desikan RSR, Busa E, Morris JC, Dale AM, Fischl B (2004): Thinning of the cerebral cortex in aging. Cereb Cortex 14:721–730.

Schlaug G (2001): The brain of musicians. A model for functional and structural adaptation. Ann NY Acad Sci 930:281–299.

Silveira M, Marques J, the Alzheimer Disease Neuroimaging Initiative (2010): Boosting Alzheimer disease diagnosis using PET images. In: 20th International Conference on Pattern Recognition. Istanbul, Turkey: IEEE. pp 2556–2559.

Stam CJ, Jones BF, Manshanden L, van Cappelen van Walsum AM, Montez T, Verbunt JPA, de Munck JC, van Dijk BW, Berendse HW, Scheltens P (2006): Magnetoencephalographic evaluation of resting-state functional connectivity in Alzheimer's disease. Neuroimage 32:1335–1344.

Stam CJ, Jones BF, Nolte G, Breakspear M, P., Scheltens (2007): Small-world networks and functional connectivity in Alzheimer's disease. Cereb Cortex 17:92–99.

Wang L, Goldstein FC, Veledar E, Levey AI, Lah JJ, Meltzer CC, Holder CA, Mao H (2009): Alterations in cortical thickness and white matter integrity in mild cognitive impairment measured by whole-brain cortical thickness mapping and diffusion tensor imaging. Am J Neuroradiol 30:893–899.

Wang L, Miller JP, Gado MH, McKeel DW, Rothermich M, Miller MI, Morris JC, Csernansky JG (2006): Abnormalities of hippocampal surface structure in very mild dementia of the Alzheimer type. Neuroimage 30:52–60.

Wechsler D (1987): WMS-R: Wechsler Memory Scale-Revised Manual. San Antonio: Psychological Corp., Harcourt Brace Jovanovich.

Wee C-Y, Yap P-T, Denny K, Browndyke JN, Potter GG, Welsh-Bohmer KA, Wang L, Shen D (2012a): Resting-state multi-spectrum functional connectivity networks for identification of MCI patients. PLoS One 7:e37828.

Wee C-Y, Yap P-T, Li W, Denny K, Browndyke JN, Potter GG, Welsh-Bohmer KA, Wang L, Shen D (2011): Enriched white matter connectivity networks for accurate identification of MCI patients. Neuroimage 54:1812–1822.

Wee C-Y, Yap P-T, Zhang D, Denny K, Browndyke JN, Potter GG, Welsh-Bohmer KA, Wang L, Shen D (2012b): Identification of MCI individuals using structural and functional connectivity networks. Neuroimage 59:2045–2056.

Whitwell JL, Crum WR, Watt HC, Fox NC (2001): Normalization of cerebral volumes by use of intracranial volume: Implications for longitudinal quantitative MR imaging. Am J Neuroradiol 22:1483–1489.

Wolf H, Grunwald M, Kruggel F, Riedel-Heller SG, Angerhofer S (2001): Hippocampal volume discriminates between normal cognition; questionable and mild dementia in the elderly. Neurobiol Aging 22:177–186.

Worsley KJ, Chen J-I, Lerch J, Evans AC (2005): Comparing functional connectivity via thresholding correlations and singular value decomposition. Phil Trans R Soc B 360:913–920.

Zanetti O, Solerte SB, Cantonni F (2009): Life expectancy in Alzheimer's disease (AD). Arch Gerontol Geriatr 49:237–243.